

Compact Dual-Passband Three-Dimensional FSS with Good Angular Stability and Both-Side Fast Roll-Off Characteristics

Zhengyong Yu^{1*}, Baozhu Li², Shenggao Ding¹, and Wanchun Tang³

¹ School of Computer and Communication
Jiangsu Vocational College of Electronics and Information, Huai'an, 223003, China
yonglly@sina.com

² Beijing National Research Center for Information Science and Technology (BNRist)
Tsinghua University
libaozhu@tsinghua.edu.cn

³ School of Electrical and Automation Engineering
Nanjing Normal University, Nanjing, 210023, China
ewwctang@nju.edu.cn

Abstract — A compact dual-passband three-dimensional (3D) frequency selective surface (FSS) is proposed based on multiple square coaxial waveguides (SCWs), which exhibits good angular stability and both-side fast roll-off characteristics. The unit cell of the proposed 3D FSS is composed of one parallel plate waveguide (PPW) propagation path and two SCW propagation paths. By etching a centered annular slot, each SCW path forms two identical short SCWs. Each short SCW inherently generates one square slot resonance. In each SCW path, on the account of electromagnetic coupling between two square slot resonators provided by two short SCWs, the square slot resonant mode will split into even-/odd-resonant modes. Accordingly, each SCW path can provide a flat second-order passband with two transmission poles. Due to the reflection and out of phase of electromagnetic waves, four transmission zeros located at both sides of the passbands are introduced for high frequency selectivity, realizing both-side fast roll-off performances. In order to explain the operating principle, the electric-field distributions at transmission-zero/pole frequencies are investigated. Finally, an FSS prototype is fabricated and measured, and the results exhibit good angular stability for both TE and TM polarizations under incident angles from 0° to 60°. In addition, the proposed 3D FSS has a compact unit cell.

Index Terms — Both-side fast roll-off, dual-passband, dual polarizations, Frequency Selective Surface (FSS), three-dimensional (3D).

I. INTRODUCTION

During the past decade, frequency selective surfaces (FSSs) have been widely investigated due to their superior

spatial filtering characteristics for some practical applications [1-4]. To meet the demands of satellite communications, dual-passband FSSs are attracting more and more attention. Dual-passband FSSs are usually realized by using complementary structure [5], convoluted structure [6], and composite structure [7]. However, these first-order dual-band FSSs in [5-7] have limitations of flatness of the passbands due to the lacking of more transmission poles. Two dual-band FSSs with one second-order passband are proposed based on shunted SIW cavity technology in [8] and multilayered cascaded technology in [9], respectively. To further promote the flatness, a dual-band FSS with second-order bandpass responses is achieved by the multi-layered array of sub-wavelength inductive wire grids and capacitive patches [10]. By using circular aperture-coupled patches, another second-order dual-passband FSS is realized in [11]. As an alternative approach, a dual-band bandpass FSS with arbitrary band ratios is designed by using three-dimensional (3D) composite topology composed of an array of three-layer parallel strip lines with inserted metallic rods, as well as two identical single-layer patch arrays [12]. Moreover, a profile, dual-band FSS with two third-order passbands is designed in [13]. Nevertheless, these FSSs in [10-13] without any transmission zeros (TZs) suffer from slow roll-off out of the passbands, resulting in poor frequency selectivity. To overcome such a limitation, a dual-band FSS with three transmission zeros is presented by utilizing a hybrid structure of double square loop slots and substrate integrated waveguide cavities, which exhibits higher frequency selectivity and passband insensitivity to the incident angles and polarizations [14]. In [15], a dual-band FSS with close band spacing is proposed by cascading a two-

layer periodic array, two transmission zeros at upper side of each passband are introduced for high frequency selectivity. With the aid of the couplings between the back-to-back annular ring resonators, a dual-band FSS with quasi-elliptic bandpass responses is realized in [16]. Unfortunately, these FSSs in [14-16] have large electrical size, leading to poor angular stability. In [17], we present a dual-passband 3D FSS with high selectivity and small band ratio based on the combination of an air-filled square waveguide and a cuboid dielectric block with double square loops, achieving good angular stability and small electrical size. However, there are no transmission zeros at the left side of the lower passbands in [14-17]. Furthermore, a via-based dual-passband 2.5D FSS is realized in virtue of electromagnetic coupling in [18], three transmission zeros are located at both sides of two passbands, exhibiting both-side fast roll-off performances, but it only operates under single polarization. Consequently, there is still a challenge for the dual-passband FSS design to achieve flat passbands, both-side fast roll-off characteristics, good angular stability, dual polarizations, and compact electrical size simultaneously.

In this paper, a compact dual-passband 3D FSS with good angular stability and both-side fast roll-off characteristics is proposed based on multiple square coaxial waveguides (SCWs). The electric-field distributions at transmission-zero/pole frequencies are analyzed for better explaining the operating principle. Finally, an FSS prototype is fabricated and measured, and its experimental results are well coincided with simulated ones.

II. UNIT CELL DESIGN AND SIMULATION

Figure 1 (a) gives the perspective view of the proposed 3D FSS, whose unit cell consists of two SCW propagation paths and one parallel plate waveguide (PPW) propagation path. These two SCW paths, namely, path 1 and path 2, are filled with dielectric 1. By etching two centered annular slots on the inner and middle tubes, each SCW path forms two identical short SCWs. The PPW path (i.e., path 3) is supported by two adjacent outer tubes combined with dielectric 2. The relative dielectric constants of the dielectric 1 and dielectric 2 are expressed as ϵ_{r1} and ϵ_{r2} , respectively. The detailed geometry is shown in Figs. 1 (b) and (c). The period and thickness of the unit cell are denoted by p and t , respectively. The parameters a , b and c represent side lengths of three tubes. The parameters s_1 and s_2 are the widths of two centered annular slots.

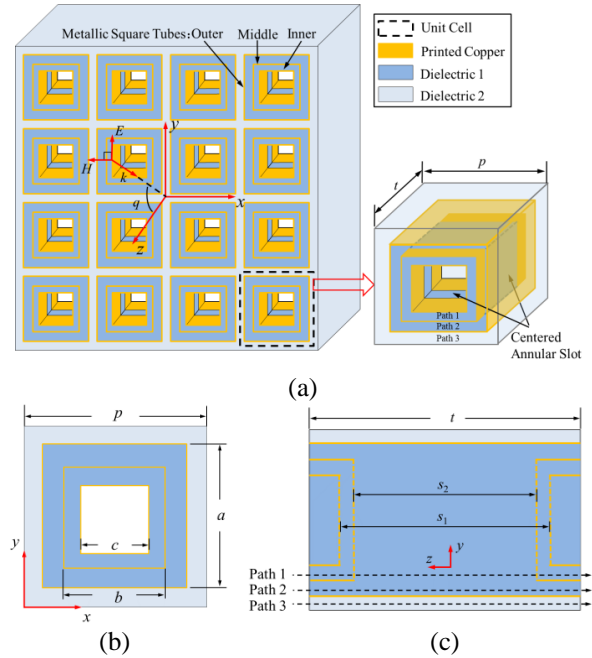


Fig. 1. Unit cell of the proposed 3D FSS: (a) perspective view, (b) top view, and (c) side view.

Figure 2 provides the simulated transmission and reflection coefficients of the presented 3D FSS by full-wave simulator HFSS. The design parameters of the proposed 3D FSS are listed in Table 1. It is observed that two flat second-order passbands are obtained around f_1 (3.55 GHz) and f_2 (5.145 GHz). In the lower band, two transmission poles are realized at f_{p1} (3.53 GHz) and f_{p2} (3.6 GHz). In the higher band, the other two transmission poles are produced at f_{p3} (5.08 GHz) and f_{p4} (5.19 GHz). Moreover, four transmission zeros at f_{z1} (3.11 GHz), f_{z2} (3.82 GHz), f_{z3} (4.65 GHz) and f_{z4} (5.82 GHz), are located at both sides of the passbands, resulting in both-side fast roll-off characteristics. As expected, its frequency selectivity is greatly improved. The 3dB bandwidths of the lower and higher bands are 0.24 GHz (3.43–3.67 GHz) and 0.41 GHz (4.94–5.35 GHz), and corresponding fractional bandwidths are 6.76% and 7.97%, respectively.

Table 1: Design parameters of the proposed 3D FSS

p	a	b	c
12 mm	11 mm	8 mm	6 mm
t	s_1	s_2	$\epsilon_{r1}, \epsilon_{r2}$
11 mm	8 mm	7.4 mm	7.5, 2.2

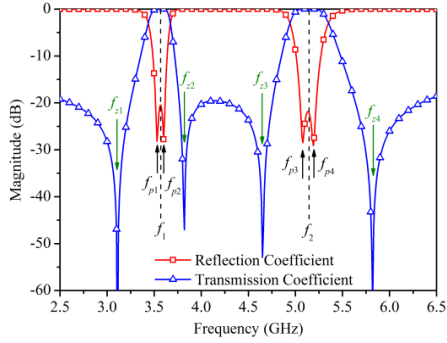


Fig. 2. Simulated transmission and reflection coefficients of the proposed 3D FSS.

III. OPERATING PRINCIPLE

Figure 3 gives the electric-field distributions at four transmission-pole frequencies. As shown in Fig. 3 (a), when the electromagnetic waves strike upon the proposed 3D FSS, the path 2 is mainly excited. From the top view, the electric-field vectors at f_{p1} are basically concentrated upon the square slots on external end-faces of the two short SCWs in path 2. From the side view, as it can be observed that the electric-field vectors reach largest value in two short SCWs in path 2, whereas the other areas become very weak, and the direction of the electric-field vectors keeps unchanged along the z -axis. As a result, f_{p1} is provided by even-resonant mode between two square slot resonators in two short SCWs, and the center location of the path 2 is equivalent to an ideal magnetic wall. At f_{p2} , the path 2 is also excited, as illustrated in Fig. 3 (b). The electric-field vectors with the same magnitude and opposite direction are distributed in two short SCWs in path 2, which reveals f_{p2} is produced by odd-resonant mode between two square slot resonators in two short SCWs, and the center location of the path 2 can be considered as an ideal electric wall. Similarly, it can be seen from Figs. 3 (c) and (d) that f_{p3} and f_{p4} are generated by even- and odd-resonant modes in path 1, respectively.

Figure 4 shows the electric-field distributions at four transmission-zero frequencies. In Fig. 4 (a), it is worth noticing that the path 2 under even-resonant mode and path 3 are excited simultaneously. The electromagnetic waves are reflected at the end of the short SCW in path 2 because of the open-end discontinuity. Additionally, the electric-field vectors in path 2 and path 3 have opposite directions at the output ports, where the electric-field vectors are combined out of phase, leading to generate one transmission zero at f_{z1} . Figure 4 (b) shows that the path 1 and path 2 under odd-resonant modes are excited at the same time. The electromagnetic waves are also reflected in path 2, and the electric-field vectors in path 1 and path 2 are combined out of phase, which provides

the other transmission zero at f_{z2} . Figures 4 (c) and (d) show the generation mechanism of the transmission zeros f_{z3} and f_{z4} respectively. The electromagnetic waves are reflected at the end of the short SCW in path 1, and the directions of electric-field vectors in path 1 and path 3 are opposite at the output ports, which contributes to the transmission zeros f_{z3} and f_{z4} .

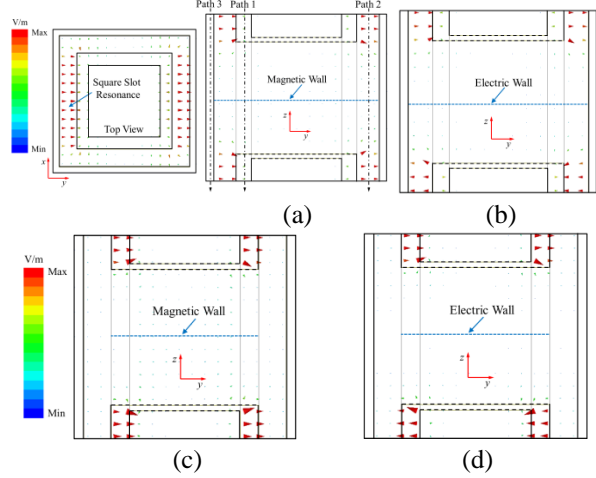


Fig. 3. Electric-field distributions at four transmission-pole frequencies: (a) f_{p1} , (b) f_{p2} , (c) f_{p3} , and (d) f_{p4} .

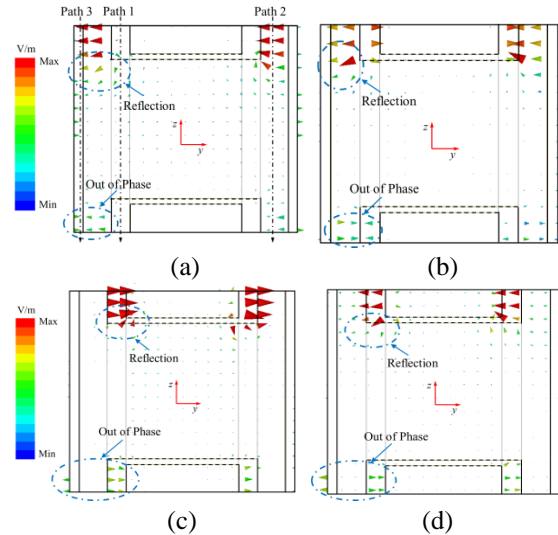


Fig. 4. Electric-field distributions at four transmission-zero frequencies: (a) f_{z1} , (b) f_{z2} , (c) f_{z3} , and (d) f_{z4} .

IV. FABRICATION AND MEASUREMENT

The fabricated FSS prototype is composed of five kinds of the building parts, as shown in Fig. 5 (a). The building part A is one piece of double sided board made of F4B material with relative permittivity of 2.2, loss tangent of 0.001 and thickness of 1.0 mm, in which 17 opening slots cut half way along the board are periodically

created. The building parts B_1 and B_2 are two types of single sided boards, which are made of TP-2 composite material ($\epsilon_r=7.5$, $\tan\delta=0.003$) with a thickness of 1.5 mm. Similarly, the building parts C_1 and C_2 are also single sided boards made of TP-2 composite material ($\epsilon_r=7.5$, $\tan\delta=0.003$) with a thickness of 1.0 mm. Each building part is manufactured by using printed circuit board technology. In Fig. 5 (b), for assembly, firstly, the pieces (part A) are cross-joined together through the opening slots to construct a frame, which achieves path 3. Subsequently, the pieces (parts B_1 and B_2) are inserted into the frame, one by one, for forming path 2. The same operation is carried out for parts C_1 and C_2 to construct path 1. Additionally, the junctions of the printed coppers are covered by conductive silver pulp for good electrical contact. Finally, the size of the fabricated 3D FSS is 213 mm \times 213 mm with 16 \times 16 (256) unit cells, as displayed in Fig. 5 (c). The electrical size of the unit cell ($p \times p \times t$) is as compact as $0.14\lambda_0 \times 0.14\lambda_0 \times 0.13\lambda_0$, where λ_0 denotes the free-space wavelength at f_1 . The free-space method is applied to obtain the frequency response of the proposed 3D FSS, and its measurement setup contains two horn antennas (from 1 to 18 GHz), one FSS prototype, one vector network analyzer, as well as one rotatable screen covered by absorbers. The FSS prototype is placed within the rectangular through-hole window in the center of the rotatable screen for the measurement of incident stability. Two horn antennas connected by the vector network analyzer are located about 1.2 m apart from each side of the centered rotatable screen. In addition, the measurement setup is surrounded by using the absorbing screens. TE or TM polarization wave is obtained when the long side of the two horn antennas is parallel or perpendicular to the ground in our measurement setup. For the transmission coefficients measurement, the propagation loss is firstly eliminated by the normalization of the measured results without the FSS, and the environment noise is eliminated by the measured results of an identically sized metallic plate. Furthermore, for considering the multipath effects, the time-domain gating function of the vector network analyzer is applied to calibrate the measured results.

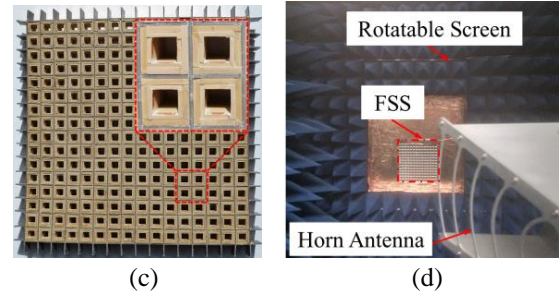
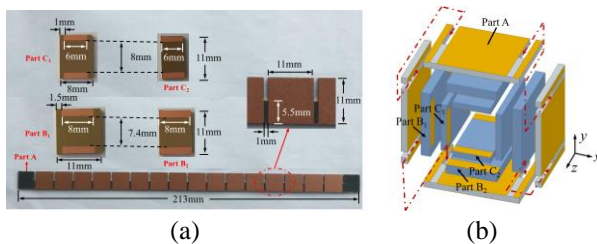
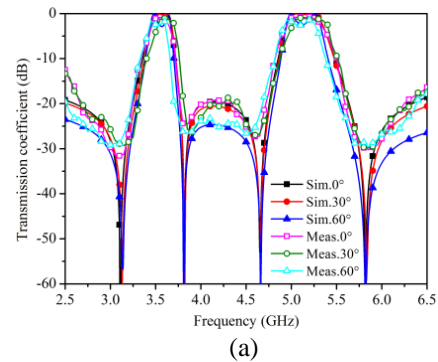


Fig. 5. Fabrication and measurement of the proposed 3D FSS. (a) Building parts and dimensions, (b) assembly process, (c) FSS prototype, and (d) measurement setup.

The measured results under different incident angles and polarizations are depicted in Fig. 6 compared with the simulated ones. It is clear that the transmission coefficients keep very stable versus variable incident angles up to 60° for transverse electric (TE) and transverse magnetic (TM) polarizations. The measured insertion losses within passbands gradually become larger as the incident angle increases, because of the variations of wave impedances for the incident waves. The measured insertion losses at the center frequency of the lower and higher bands are 0.8 and 1.0 dB under the normal incidence, respectively, which are larger than the simulated ones. It results from the conductor losses unconsidered in the simulated model. The other discrepancies between the measurement and simulation result from fabrication tolerance, assembly tolerance and measurement error. However, the measured results have demonstrated the desired performances of the proposed 3D FSS. Table 2 shows the comparison between the presented FSS and recently published researches with similar performances. Obviously, the proposed 3D FSS has an overwhelming advantage in flat passbands, both-side fast roll-off characteristics, good angular stability, dual polarizations, and compact unit cell.



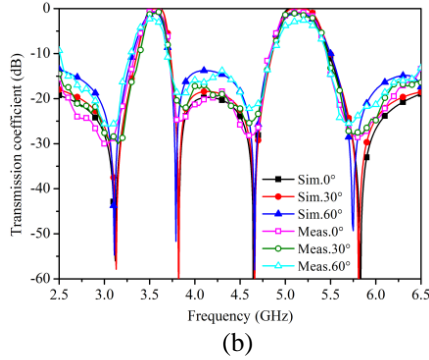


Fig. 6. Measured and simulated results of the proposed 3D FSS. (a) TE polarization. (b) TM polarization.

Table 2: Comparison of the FSS designs with similar responses

Ref.	Unit Cell Size and Thickness	TZs Num.	Polarization	Angular Stability (TE/TM)
[10]	$0.094\lambda_0 \times 0.094\lambda_0 \times 0.23\lambda_0$	0	Dual	$45^\circ/45^\circ$
[11]	$0.495\lambda_0 \times 0.495\lambda_0 \times 0.05\lambda_0$	0	Dual	$30^\circ/30^\circ$ (only sim.)
[12]	$0.07\lambda_0 \times 0.055\lambda_0 \times 0.09\lambda_0$	0	Single	40°
[14]	$0.49\lambda_0 \times 0.49\lambda_0 \times 0.032\lambda_0$	3	Dual	$30^\circ/30^\circ$
[15]	$0.37\lambda_0 \times 0.37\lambda_0 \times 0.22\lambda_0$	4	Dual	$45^\circ/45^\circ$
[16]	$0.38\lambda_0 \times 0.38\lambda_0 \times 0.135\lambda_0$	4	Dual	$30^\circ/30^\circ$
[17]	$0.188\lambda_0 \times 0.188\lambda_0 \times 0.094\lambda_0$	4	Dual	$60^\circ/60^\circ$
[18]	$0.27\lambda_0 \times 0.096\lambda_0 \times 0.03\lambda_0$	3	Single	60° (only sim.)
This work	$0.14\lambda_0 \times 0.14\lambda_0 \times 0.13\lambda_0$	4	Dual	$60^\circ/60^\circ$

V. CONCLUSION

A compact, dual-polarized, dual-passband 3D FSS, exhibiting good angular stability and both-side fast roll-off characteristics, has been presented based on multiple SCWs. Thanks to the electromagnetic coupling between two square slot resonators provided by two short SCWs in the SCW path, each SCW path can provide a flat second-order passband. Four transmission zeros are introduced for realizing both-side fast roll-off performances with the aid of the reflection and out of phase of electromagnetic waves. For explaining the operating principle of the proposed 3D FSS, the electric-field distributions at the frequencies of the transmission zeros/poles are investigated. Finally, an FSS prototype is fabricated and measured. The consistency between measurement and simulation validates our design.

ACKNOWLEDGMENT

This work was supported by Doctor Studio Project, Qing Lan Project, RF Integrated Circuits and Systems Innovation Team (No. JSEIYC2020002), Natural Science Foundation of the Jiangsu Higher Education Institutions of China (No. 19KJB510002), “333 Project” Research Funding Project of Jiangsu Province (No. BRA2018315), National Natural Science Foundation of China (No. 61571232) and Huai’an Innovation Service Capacity Construction Project (HAP201904).

REFERENCES

- [1] B. A. Munk, *Frequency Selective Surfaces: Theory and Design*. New York, NY, USA: Wiley, 2000.
- [2] M. Y. Wang, L. Zhao, J. Wang, X. H. Liang, S. J. Zhang, Y. S. Li, and W. H. Yu, “A low-profile miniaturized frequency selective surface with insensitive polarization,” *Applied Computational Electromagnetics Society Journal*, vol. 33, no. 9, pp. 1003-1008, 2018.
- [3] M. Idrees, S. Buzdar, S. Khalid, and M. A. Khalid, “A miniaturized polarization independent frequency selective surface with stepped profile for shielding applications,” *Applied Computational Electromagnetics Society Journal*, vol. 31, no. 5, pp. 531-536, 2016.
- [4] W. X. Li, C. M. Wang, Y. Zhang, and Y. S. Li, “A miniaturized frequency selective surface based on square loop aperture element,” *International journal of antennas and propagation*, vol. 2014, article ID 701279, 2014.
- [5] X. Hu, X. Zhou, L. Wu, L. Zhou, and W. Yin, “A miniaturized dual-band frequency selective surface (FSS) with closed loop and its complementary pattern,” *IEEE Antennas Wireless Propag. Lett.*, vol. 8, pp. 1374-1377, 2009.
- [6] P. Zhao, Z. Zong, W. Wu, and D. Fang, “A convoluted structure for miniaturized frequency selective surface and its equivalent circuit for optimization design,” *IEEE Trans. Antennas Propag.*, vol. 64, no. 7, pp. 2963-2970, 2016.
- [7] S. Yadav, C. P. Jain, and M. M. Sharma, “Polarization independent dual-bandpass frequency selective surface for Wi-Max applications,” *Int. J. RF Microw. Comput. Aided Eng.*, vol. 28, no. 6, pp. e21278, 2018.
- [8] V. Krushna Kanth and S. Raghavan, “Dual-band frequency selective surface based on shunted SIW cavity technology,” *IEEE Microwave and Wireless Components Letters*, vol. 30, no. 3, pp. 245-248, 2020.
- [9] A. Chatterjee and S. K. Parui, “A triple-layer dual-bandpass frequency selective surface of third order response with equivalent circuit analysis,” *Int. J. RF Microw. Comput. Aided Eng.*, vol. 30, no. 2, pp. e22047, 2020.
- [10] M. Gao, S. M. A. M. H. Abadi, and N. Behdad,

“A dual-band, inductively coupled miniaturized-element frequency selective surface with higher order bandpass response,” *IEEE Trans. Antennas Propag.*, vol. 64, no. 8, pp. 3729-3734, 2016.

- [11] H. Zhou, S. B. Qu, B. Q. Lin, J. Q. Zhang, C. Gu, H. Ma, Z. Xu, P. Bai, and W. D. peng, “Dual band frequency selective surface based on circular aperture-coupled patches”, *Microw. Opt. Technol. Lett.*, vol. 53, no. 8, pp. 1784-1786, 2011.
- [12] B. Li and Z. Shen, “Dual-band bandpass frequency-selective structures with arbitrary band ratios,” *IEEE Trans. Antennas Propag.*, vol. 62, no. 11, pp. 5504-5512, 2014.
- [13] G. Xu, G. V. Eleftheriades, and S. V. Hum, “Generalized synthesis technique for high-order low-profile dual-band frequency selective surfaces,” *IEEE Trans. Antennas Propag.*, vol. 66, no. 11, pp. 6033-6042, 2018.
- [14] G. Q. Luo, W. Hong, H. J. Tang, J. X. Chen, and K. Wu, “Dualband frequency-selective surfaces using substrate-integrated waveguide technology,” *IET Microw. Antennas Propag.*, vol. 1, no. 2, pp. 408-413, 2007.
- [15] M. B. Yan, J. F. Wang, S. B. Qu, M. D. Feng, Z. Q. Li, H. Y. Chen, J. Q. Zhang, and L. Zheng, “Highly-selective, closely-spaced, dual-band FSS with second-order characteristic,” *IET Microw. Antennas Propag.*, vol. 10, no. 10, pp. 1087-1091, 2016.
- [16] B. Zhang, C. Jin, X. Ye, and R. Mittra, “Dual-band dual-polarized quasi-elliptic frequency selective surfaces,” *IEEE Antennas Wireless Propag. Lett.*, vol. 18, no. 2, pp. 298-302, 2019.
- [17] Z. Yu, X. Yang, J. Zhu, C. Wang, Y. Shi, and W. Tang, “Dual-band three-dimensional FSS with high selectivity and small band ratio,” *Electron. Lett.*, vol. 55, no. 14, pp. 798-799, 2019.
- [18] S. Yang, Q. Chen, J. Bai, and Y. Fu, “Design of ultra-thin closely spaced dual-band bandpass frequency selective surface,” *Electron. Lett.*, vol. 53, no. 24, pp. 1583-1585, 2017.



Zhengyong Yu was born in Huaian, China, in 1982. He received the B.S. degree from the Huaiyin Institute of Technology, Huaian, China, in 2006, the M.S. degree from the Nanjing University of Science and Technology, Nanjing, China, in 2008, and the Ph.D. degree from Nanjing

Normal University, in 2020.

He is currently an Associate Professor and Senior Engineer in Jiangsu Vocational College of Electronics and Information. He is Jiangsu Province 333 project personnel training object, and Jiangsu Province Qing Lan Project Academic Leader. His current research

interests include fundamental electromagnetic theory, frequency selective surfaces and near-field antennas.



Baozhu Li was born in Henan Province, China, in 1990. She received the B.S. degree in Electrical Engineering from Nanjing Normal University Zhongbei College, Nanjing, in 2013, and the Ph.D. degree in Physical Electronics from School of Physics and Technology, Nanjing Normal University, in 2020. She was a Visiting Ph.D. Student funded by Scholarship Council in ELEDIA Research Center at University of Trento, Italy, from Sep. 2018 to Jan. 2020.

She is currently a Postdoctoral Researcher in Beijing National Research Center for Information Science and Technology at Tsinghua University and an Associate Faculty Member of the ELEDIA Research Center. Her research interests include electromagnetic environment and inverse propagation problems.



Shenggao Ding was born in Huaian, China, in 1980. He received the B.S. degree from the North China Electric Power University, Baoding, China, in 2002, the M.S. degree from the Nanjing University of Posts and Telecommunications, Nanjing, China, in 2006. He was a Visiting

Scholar with the University of South Carolina, Columbia, USA, from 2019 to 2020.

He is currently a Lecturer in Jiangsu Vocational College of Electronics and Information. His current research interests include RF and Microwave Components/Circuits for Wireless Communications, 5G Mobile Antennas and Internet of Things.



Wanchun Tang was born in China in 1967. He received the B.S. degree from Tsinghua University, Beijing, China, in 1990, the M.S. degree from the Nanjing University of Science and Technology, Nanjing, China, in 1995, and the Ph.D. degree from the City University of Hong Kong, Hong Kong, in 2003, all in Electrical Engineering.

He was a Full Professor with the Department of Communication Engineering, NJUST, and is currently a Specially Invited Full Professor with the Jiangsu Key Laboratory on Optoelectronic Technology, School of Physics and Technology, Nanjing Normal University, Nanjing. He has authored or coauthored over 100 journal and conference papers. His current research interests include modeling and optimization of RFIC, antennas, signal integrity, and power integrity design in package.